On velocity profiles and stresses in sheared and vibrated granular systems under variable gravity

Oleh Baran[a] and Lou Kondic[b]
Department of Mathematical Sciences and Center for Applied Mathematics and Statistics, New Jersey Institute of Technology, Newark, New Jersey 07102

(Received 5 May 2006; accepted 19 July 2006; published online 8 December 2006)

We employ discrete element three-dimensional simulations that include realistic modeling of physical system boundaries to determine the influence of gravity on velocity profiles and stresses for frictional inelastic particles that are confined in an angular Couette cell, and sheared by a rotated upper wall. In addition to Earth gravity, we consider other gravitational fields, in particular those of the Moon and Mars. The computational techniques are based on hard-sphere simulations of polydisperse particles at relatively high volume fraction (50–55%). We find that the presence of gravity induces significant changes of the velocity profiles and stresses. One important nondimensional parameter in the problem is shown to be $I_\Omega = \dot{\gamma} d / \sqrt{P_g / \rho_s}$, where $\dot{\gamma}$ is the imposed shear rate, P_g is the weight of the system per unit area due to gravity, and ρ_s is the solid density. We also consider systems that are vibrated in addition to being sheared, since vibrations are one of several important methods for agitating (e.g., fluidizing and/or unjamming) granular systems. We find that the introduction of nondimensional acceleration $\Gamma = a(2\pi f)^2/g$, where a, f, g are the amplitude and frequency of oscillations, and the acceleration of gravity, explains novel features that develop in these complex granular systems. © *2006 American Institute of Physics*.
[DOI: 10.1063/1.2397007]

I. INTRODUCTION

There has been a significant amount of work on the response of granular systems to shear, including experiments,[1] continuous models,[2,3] and simulations,[4–6] to mention just a few examples. The same can be said about granular systems subjected to external vibrations. However, granular flow with both shearing and oscillations has neither been well studied nor understood. These granular systems have great potential in industrial applications, because it is thought that vibrations under the right conditions can enhance granular flow. An example is the successful use of "bin activators" in hopper flows to prevent jamming.[7] At the same time, vibrations are known to affect the flow in ways that may differ significantly depending on the strength of the vibrations and other conditions. For example, without shear, highly vibrated granular systems become fluid- or gas-like, while tapping-type vibrations in gravity cause the system to compact.[8,9] In the presence of shear, an interaction of different effects may lead to a variety of behaviors. For example, very recently, Daniels and Behringer[10] studied granular flow in an annular cell sheared from above and vibrated from below and discovered a novel "freezing-by-heating" phase transition. More generally, systematic characterization of sheared and vibrated systems could be very helpful in developing a continuum theory of granular flows. We expect that the results reported here will be useful for further research in this direction.

One of the important questions in shear flows (either with oscillations or without them) is the stress dependence on external driving and other properties of the granular systems. In a zero g (gravity) environment, it has been found that, under a wide range of conditions, the stresses scale with the square of the imposed shearing velocity, v; see, for example, Ref. 11. This scaling was also observed under gravity in the "rapid flow" regime.[12] The scaling is different, however, under gravity for slower shear rates.[4,12,13] There have been attempts to unify the factors influencing the rheology and stress scaling of sheared granular flow using one or more dimensionless quantities. For example, Campbell[4] suggests that the dimensionless combination of stiffness of grains and shear rate is responsible for the different flow regimes observed in simulations. Recently, daCruz *et al.*[14] recognized the importance of applied stress on the flow regimes and introduced the dimensionless number, I, which is the ratio of inertial to pressure forces. Similar arguments were discussed in Ref. 15. These arguments were, however, illustrated only in application to two-dimensional (2D) systems in zero gravity where the boundary effects were significantly minimized. Clearly, to account for gravity, a dimensional control parameter should depend on the gravitational acceleration, g. This idea was used in Refs. 10, 12, and 16 to define a dimensionless shear rate to correlate experimental results. These experimental results were, however, limited to Earth gravity, and cannot directly confirm the relevance of the proposed dimensionless number as g is varied. Numerical simulations, as used in our work, seem to be the most suitable approach to establish this scaling.

In this work, we discuss the influence of gravity and external vibrations on both the velocity profiles and the

[a]Present address: ExxonMobil Research and Engineering, 1545 Route 22 East, Annandale, NJ 08801.
[b]Electronic mail: kondic@njit.edu; http://m.njit.edu/~kondic/

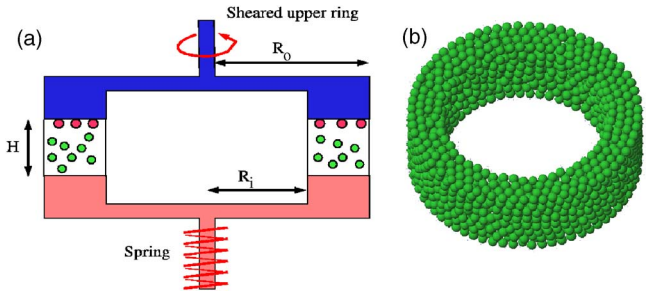

FIG. 1. (Color online) Geometry of the flow (a) and a snapshot of the system particles (b).

stresses in a sheared angular Couette cell via discrete element 3D simulations (DES) that include realistic modeling of the physical system boundaries (walls). In addition to Earth gravity ($g=981$ cm/s^2), we consider other values of gravity, in particular the gravitational fields of the Moon ($g=162$ cm/s^2) and Mars ($g=373$ cm/s^2). These gravities are of interest for space exploration and are one of the primary motivations for our research. Lower gravities can, however, provide a useful link between zero gravity and higher gravity results. For this reason, we also report the results for both zero gravity and $g=50$ cm/s^2. More details regarding zero g results can be found in our earlier work.[6]

II. SIMULATED SYSTEM AND NUMERICAL METHOD

Figure 1(a) shows the geometry of the flow considered, and Fig. 1(b) shows a snapshot of the particle positions (with the boundaries removed). We simulate $N=2000$ particles that are confined in an angular Couette cell. The computational techniques are based on hard-sphere simulations at relatively high values of the volume fractions, ν, i.e., $\nu \approx 50\%$. The particles are polydisperse with diameters randomly distributed in the range $[0.9,1.1]\,d$, where $d=0.1$ cm is the average diameter of particles and is used in what follows as the characteristic length scale. The particle interactions are characterized by three parameters: (i) the coefficient of friction μ; (ii) the velocity-dependent coefficient of restitution $e(v_n)$; and (iii) the coefficient of tangential restitution β, defined as the ratio of the tangential components of the relative velocity after and before collision. The coefficient of friction between the particles is set equal to 0.5 for all of our simulations. The coefficient of restitution $e(v_n)$ is calculated for each collision as[6,17]

$$e(v_n) = \begin{cases} 1 - Bv_n^{3/4}, & v_n < v_0, \\ \epsilon, & v_n > v_0, \end{cases} \tag{1}$$

where v_n is the component of relative velocity along the line joining particle centers, $B=(1-\epsilon)v_0^{(-3/4)}$, $v_0 \simeq 100$ cm/s, and ϵ is a restitution parameter. The coefficient of tangential restitution, β, is given by[6,18]

$$\beta = \begin{cases} -1 + \frac{7}{2}\mu(1+e)v_n/v_t & \text{for sliding contacts,} \\ \beta_0 & \text{for rolling contacts,} \end{cases} \tag{2}$$

where v_t is the component of relative velocity in the plane perpendicular to v_n (i.e., the tangential relative velocity) and β_0 is the rotational restitution parameter, which also determines the transition between rolling and sliding contacts. As in Ref. 6, we use $\epsilon=0.6$ and $\beta_0=0.35$.

Particles settle under gravity and we find that the smallest value of the volume fraction for which the particles shear is about 52%. Even for these volume fractions, a significant wall velocity is needed to induce shear within the granular pack.[19]

The bottom wall of the cell may be either stationary or vertically oscillating, and it is assigned a very high coefficient of friction, $\mu_{\text{bottom}}=0.9$. The top wall is rotating and has superimposed upon it additional roughness in order to increase shear. To improve the computational efficiency, we model the effect of the top wall roughness by a simplified particle-wall interaction model where the rebound velocity of the particles is first calculated in a usual way, and then the horizontal components of the rebound velocity are set to the values of top wall velocity at the point of contact.[20,21] This is expected to model well the conditions when the top wall is roughened by particles glued to the surface. We confirmed the applicability of this approach by comparing the results with those obtained by direct simulation of particles glued to the top wall.[6]

The inner and outer boundaries of the cell are stationary and have radii $R_i/d=8$ and $R_o/d=12$, respectively. These sidewalls are given a friction coefficient $\mu_{\text{sidewall}}=0.1$ and they are more elastic, $\epsilon=0.9$. We set the height of the cell to $H/d=8$, which sets the mean volume fraction to $\nu=52\%$. As mentioned above, we also simulate systems in which the bottom wall is vibrated vertically. In this case, the vertical y component of the bottom wall position follows the sinusoidal rule, $y=a\sin(2\pi ft)$.

The initial conditions are prepared by first generating N particles in zero gravity with random initial velocities inside the cell of extended height. The bottom wall is then set in slow motion toward the rotating top wall until the desired volume fraction is obtained. At this point, the coordinates of all particles are recalculated with respect to the reference origin at the center of the bottom wall. Next, the gravity and shear velocity are adjusted to the desired values, and the bottom wall oscillations are set if needed. The system is then sheared for a relatively long time (typically 10 s for the system without oscillations and 3 s for the systems with oscillations) until steady state is obtained. In some cases, we perform simulations for much longer times to verify the steadiness of the results.

III. VELOCITY PROFILES AND STRESSES WITHOUT OSCILLATIONS

In the simulations, shear within the grain pack is driven by rotation of the upper wall with angular velocity Ω (in units of rad/s). Figure 2 shows the angular velocity profiles,

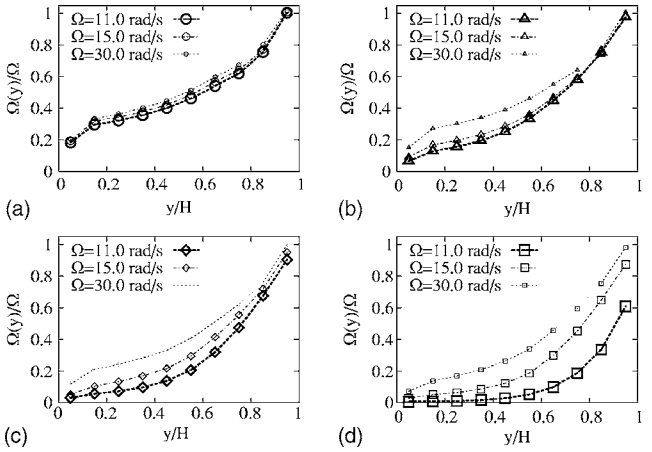

FIG. 2. Velocity profiles for different Ω's and for (a) zero g, (b) Moon gravity ($g=162$ cm/s^2), (c) Mars gravity ($g=373$ cm/s^2), and (d) Earth gravity ($g=981$ cm/s^2). The shearing wall is at $y/H=1$.

in which $\Omega(y)$ is normalized by the value imposed at the top surface and y is a distance from the bottom.

Velocity profiles in a zero g environment are shown in Fig. 2(a). The profiles are approximately linear with some slip close to the bottom boundary. Unlike the results for 40% volume fraction considered in our earlier work,[6] the profiles show a rather weak dependence on the shearing velocities. This difference occurs because in the case of the relatively large (52%) volume fraction considered here, the fraction of the energy dissipation within that grain pack is much larger than that at sidewalls, thereby minimizing the effect of these boundaries on the velocity profiles. In Ref. 6, we showed that for 40% volume fraction, the sidewall friction was the main reason for imperfect scaling of velocity profiles, leading to lower scaled velocities at lower shearing.

The rest of Fig. 2 concentrates on the flow under gravity. We can clearly see how the velocity profiles change from approximately linear to approximately exponential (shear banded) with the stronger curvature of the profiles appearing for larger g's and smaller Ω's. This effect leads to shear rate dependence of the velocity profiles in the sense that the scaled shear velocities do not scale with the imposed shear.

Next, we concentrate on the normal and shear stresses on the bottom boundary. To obtain an average stress, we calculate first the "instantaneous" stress resulting from the momentum exchange during collisions between particles and the bottom wall over some averaging time Δt,

$$\sigma_{\alpha\beta} = \frac{1}{A_s \Delta t}\frac{1}{6}\pi\rho_s \sum_i d_i^3 \Delta v_{\alpha\beta}. \tag{3}$$

Here $\alpha\beta$ is either yy for the normal direction or xy for the tangential (shear) direction. ρ_s is the density of the solid material, d_i is the diameter of a particle participating in the collision i, and $\Delta v_{\alpha\beta}$ is the change of an appropriate component of velocity during a collision. The sum runs over all collisions between the particles and the bottom wall area $A_s=\pi(R_o^2-R_i^2)$ during Δt. In order to obtain enough data for stress distributions, we set Δt to a small value that still includes a relatively large number of contacts between the wall and the particles. The typical value $\Delta t=0.0027$ s used in Ref. 6 satisfies the above requirements, and we use it here. These "instantaneous" stresses are subsequently averaged over a longer time period (typically 2 s), leading to an average stress on the bottom boundary that we report in what follows.

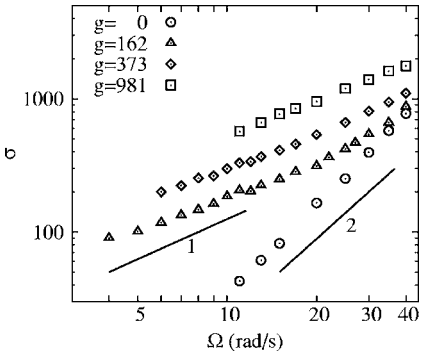

FIG. 3. Average normal stresses $\sigma=\sigma_{yy}$ (in units of $\rho_s$cm^2/s^2) on the bottom wall for four different gravities. The line segments of slopes 1 and 2 illustrate the stress scaling.

Figure 3 shows the average normal stress $\sigma=\sigma_{yy}$ on the bottom wall versus Ω for four values of g (the solid lines on this log-log plot correspond to the slopes 1 and 2). Therefore, for $g=0$ (open circles), we find a quadratic scaling of the normal stresses with Ω, in agreement with Bagnold.[11] This is also consistent with the results reported in Ref. 6. However, the results for nonzero gravities show significant qualitative differences compared to the zero g results. For nonzero g we observe *linear* or close to linear scaling of the stresses; therefore, gravity significantly modifies the stress scaling. We note that stress scaling of the form $\sigma \propto \Omega^n$, with $n \approx 1$ in the presence of gravity, was also reported in Refs. 12 and 16. We also note that we do not observe any hysteretic effects in our simulations, i.e., the reported stress values are independent of whether one moves up or down the stress curves shown in Fig. 3. Hysteretic effects have been reported in some experiments[16] performed with similar volume fractions; however, the nonunique stress states in these experiments were mostly interpreted by aging of the granular particles.

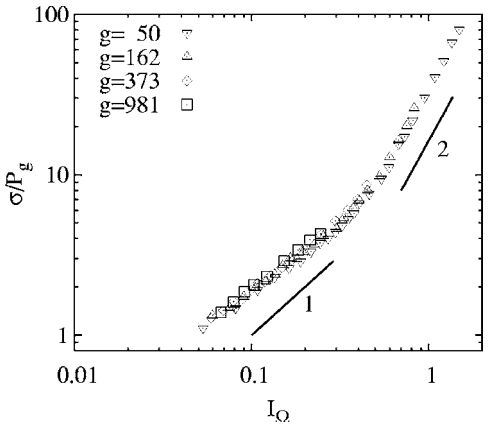

FIG. 4. Dimensionless stress versus I_Ω. The line segments have slopes 1 and 2.

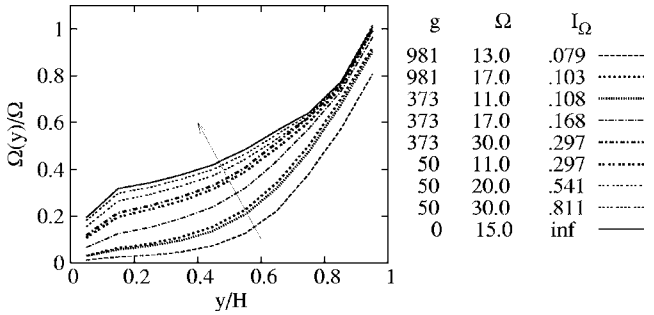

FIG. 5. Scaled velocity profiles for different values of I_Ω shown in the legend. The arrow shows the direction of increased I_Ω.

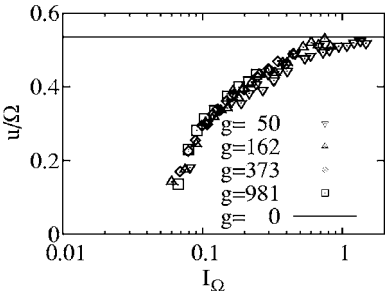

FIG. 6. Vertically averaged scaled velocity versus I_Ω for nonzero gravities. Note that zero g also corresponds to the limiting case of infinite I_Ω.

We note in Fig. 3 that for Moon gravity, presented by the triangles, there appears an indication of turning from linear to quadratic scaling for high Ω. This transition is absent from the Mars and Earth gravity results, at least for the shown shearing velocities. This observation suggests that both gravity and shearing affect the scaling. Therefore, we expect that a dimensionless combination of g and Ω is a relevant control parameter. Similarly to Refs. 14, 15, and 22, we introduce the dimensionless inertial number

$$I_\Omega = \frac{\dot{\gamma} d}{\sqrt{P_g/\rho_s}}. \tag{4}$$

Here $\dot{\gamma}=\Omega R/H$ is an applied shear rate, where $R=\frac{1}{2}(R_i+R_o)$ is an average radius of the Couette cell and H is its height; see Fig. 1. P_g is defined to be equal to the stress due to the gravitational weight of the system, $P_g=\nu\rho_s gH$. Therefore, the inertial number I_Ω describes the relative importance of inertia and gravity. This number is different from the $I\equiv\dot{\gamma}d/\sqrt{(\sigma_{yy}/\rho_s)}$ used, for example, in Ref. 15. First, it is a global quantity. Second, it depends on the gravitational weight P_g and not on the applied stress σ_{yy}. In fact, the relation between I_Ω and the global version of I is the following: $I_\Omega/I=\sqrt{\sigma_{yy}/P_g}$. Our definition of I_Ω is also closely related to the dimensionless shear rate $\dot{\gamma}^*$ used by Savage and Sayed[16] and Tardos *et al.*,[12] $\dot{\gamma}^*\equiv\dot{\gamma}/\sqrt{g/d}=I_\Omega\sqrt{\nu H/d}$. Similarly, it is closely related to the dimensionless shear $\tilde{\Omega}$ used by Daniels and Behringer,[10] $\tilde{\Omega}=(\sqrt{\nu}/2\pi)(H/d)^{(3/2)}I_\Omega$.

Figure 4 shows the scaled stress σ/P_g versus I_Ω. In addition to the data presented in the preceding figure, this figure includes the results of additional simulations performed using different values of Ω, and one additional value of $g=50$ cm/s^2 (this small value of g will help us understand the transition between zero g and large g). The first and most important observation in Fig. 4 is that I_Ω is an excellent parameter to describe the flow, since the results obtained for all values of the gravity and shear rate collapse onto a single curve. We will see in the rest of this section that the collapse of the data occurs for other flow variables as well. In addition, Fig. 4 shows that, for our system, there exists a critical value of $I_\Omega\simeq 0.7$ at which the scaling changes from linear to quadratic.

An obvious question to ask is whether there is a connection between the transition in stress scaling (from quadratic to linear) and in the velocity profiles (from linear to exponential/shear banded). To help answer this question, Fig. 5 shows the velocity profiles for four values of g (g=981, 373, 50, and 0 cm/s^2), and for various values of Ω. We immediately note that the profiles characterized by similar values of I_Ω lay almost on the top of each other [e.g., the profile obtained using $(g,\Omega)=(373,30)$ practically coincides with the one resulting from $(g,\Omega)=(50,11)$, and $(g,\Omega)=(981,17)$ coincides with $(g,\Omega)=(373,11)$]. Furthermore, the larger the value of I_Ω is , the smaller is the curvature of the profiles. Therefore, the value of I_Ω can be directly used to distinguish between approximately linear and approximately exponential/shear banded velocity profiles. However, we do not observe a sharp change in the shapes of velocity profiles as we go from the regime with linear ($I_\Omega<0.7$) to quadratic ($I_\Omega>0.7$) stress scaling.

Another quantity of interest is the vertically averaged velocity, u, which is easily measured in experiments since it is directly related to the total mass flux.[23] This quantity reflects the cumulative effect of slip velocities at the boundaries and curvature of the velocity profiles, and it is defined by

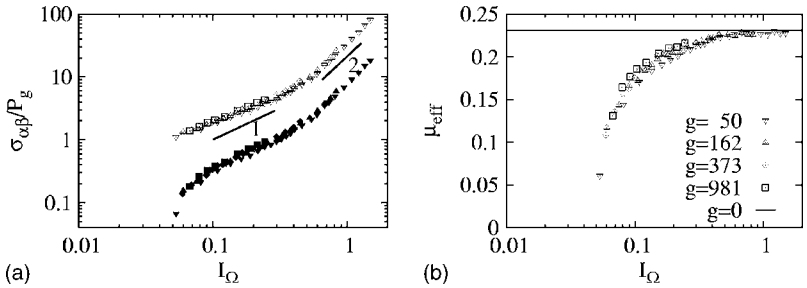

FIG. 7. (a) Normal (hollow symbols) and shear (filled symbols) stress for Moon gravity (g=162 cm/s^2) and (b) the ratio of shear to normal stress, μ_{eff}, for all nonzero gravities (symbols) in comparison to the zero g ratio (solid line).

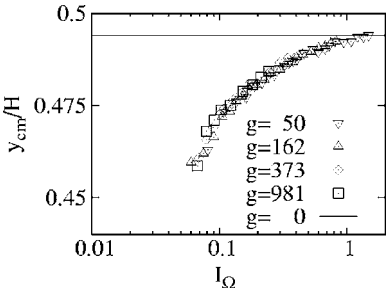

FIG. 8. y position of the center of mass of all particles. Solid line indicates the average value of y_{cm}/H in zero gravity.

$$u = \frac{1}{H}\int_0^H \Omega(y)dy. \tag{5}$$

Figure 6, where u/Ω is plotted versus I_Ω, shows that the results for different gravities collapse onto a single curve, illustrating again that I_Ω is an appropriate parameter to describe the flow. This curve is flattening for $I_\Omega \approx 1$ at the level of the average velocity obtained under zero g. The direct connection between the flow velocity u and the inertial number I_Ω makes an important link between u and any other macroscopic quantity that uniquely depends on I_Ω.

Next we consider the connection between the shear, σ_{yx}, and normal, σ_{yy}, stresses. Figure 7(a) illustrates the dependence of these quantities on I_Ω for Moon gravity. Qualitatively, both stresses show a similar scaling transition at $I_\Omega \simeq 0.7$. However, the effective friction coefficient of the flow, defined as the ratio of the shear to normal stress, $\mu_{eff}=\sigma_{yx}/\sigma_{yy}$ and shown in Fig. 7(b), is increasing in the linear regime and is almost constant in the quadratic regime. This figure, in which we also present the results obtained using other values of g, shows that this behavior is generic. This result is related to the "friction law" discussed in Ref. 14 (see Fig. 3 of that reference). We note in passing that similar collapse of the ratio of shear to normal stresses to a single curve is also observed at the upper wall.

Figure 8 shows the effect of I_Ω on the position of the center of mass of all particles with respect to the bottom wall, $y_{cm}=\Sigma_i^N y_i/N$. We note again very good collapse of the data when presented as a function of I_Ω. To explain the results shown in Fig. 8, we note that the effect of shear caused by the upper wall is to form a dilation zone there. For low I_Ω, this dilation combined with gravity effects leads to a shift of y_{cm} to smaller values of y. As I_Ω increases, however, the amount of shear throughout the system increases (viz. Fig. 2) and the particles tend to retract from the bottom wall, leading to an increase of y_{cm}.

Finally, the distributions of the normal stress on the bottom wall are shown in Fig. 9. The distributions $P(\sigma)$ are obtained from statistical analysis of the instantaneous stresses (3) collected every Δt seconds over a long time period. We notice almost no effect of gravity and shearing velocity on the shape and width of distribution of $\sigma/\langle\sigma\rangle$, although there is some weak narrowing of the distributions for smaller values of I_Ω and/or for larger gravities. Therefore, the width of the normal stress distribution is approximately proportional to the average normal stress in both the linear and quadratic regimes.

We note that in our earlier work,[6] where we considered a system of smaller volume fraction, 40%, the width of the stress distributions was found to depend on Ω for smaller Ω's. In the case considered here (ν=52%), the system is less compressible and the effect of the shearing wall is much stronger. Therefore, the quasistatic features of the flow (such as broadening of stress distribution) should appear at values of the shear velocity lower than the ones considered and are not seen in Fig. 9.

IV. VELOCITY PROFILES AND STRESSES WITH OSCILLATIONS

Next we consider the effect of oscillations of the bottom boundary on the system properties. These oscillations are often used in laboratory experiments to help fluidize the

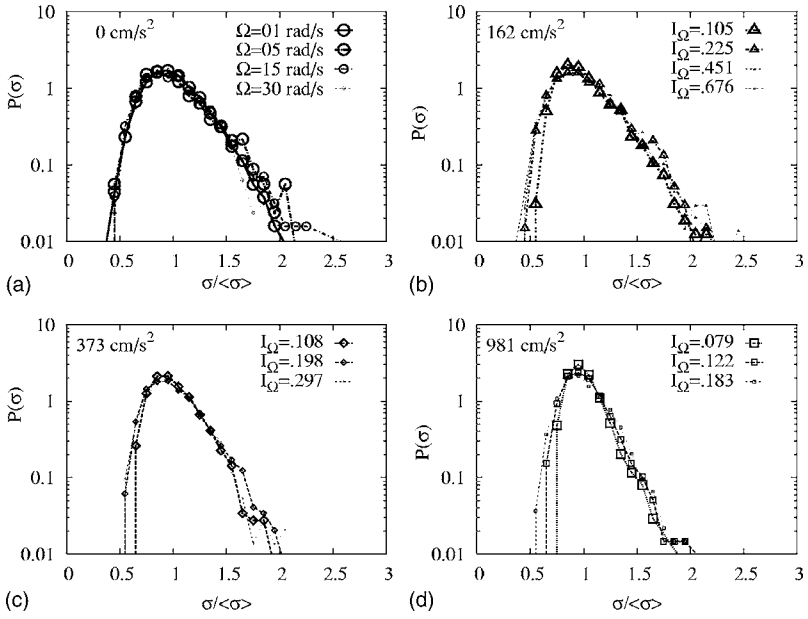

FIG. 9. Normal stress distributions for different gravities (shown in the upper left corner of each figure). Here $\langle\sigma\rangle$ is the average stress for a given (g,Ω) pair.

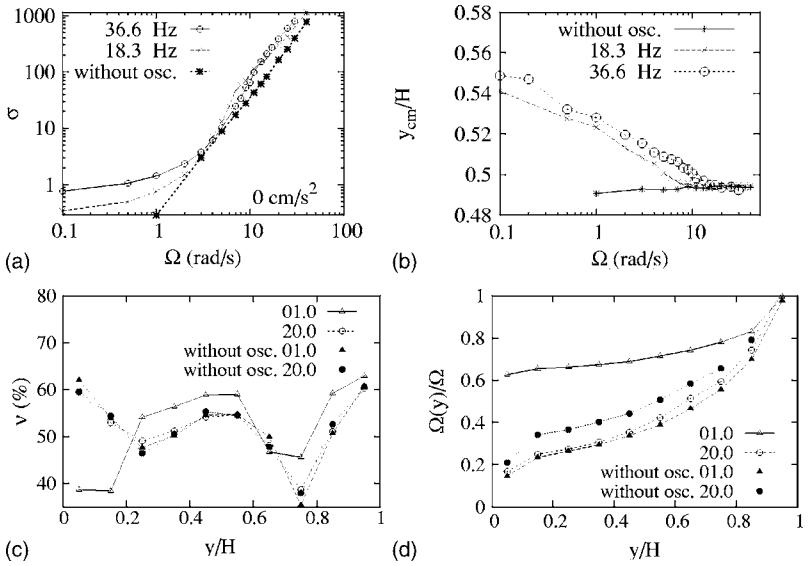

FIG. 10. Comparison of the results with and without oscillations for the system in zero g. (a) Normal stress and (b) y position of the center of mass versus Ω for two frequencies of oscillations. (c) Volume fraction and (d) velocity profiles versus distance from the shearing wall for low ($\Omega=1$ rad/s) and high ($\Omega=20$ rad/s) shearing ($f=36.6$ Hz here).

granular flow and enhance shearing. They are also present, and may impact the flow, in situations in which they are not purposefully generated and/or controlled, for example the vibrations induced by running nearby machinery, earthquakes, etc. Therefore, it is of considerable interest to explore how the interplay between oscillations, shear, and gravity determines the granular dynamics.

We have performed simulations in which the bottom wall is oscillated with an amplitude equal to $0.1d$ and various frequencies ($f=36.6$ Hz is used if not specified otherwise). In order to average out the periodic component in the stress due to these oscillations, here we set Δt in Eq. (3) to the value of the period of oscillation, $\Delta t=2\pi/f$. The systems described in what follows are equilibrated for a range of Ω's by taking the corresponding nonoscillating state as an initial state. We have confirmed that the same final steady state is obtained for different initial configurations. For example, the same final state results if we start from an initial state obtained with oscillations at low shear and then gradually increase the shear velocity, or if we start from the high-shear state and then decrease the shear velocity. We discuss the effect of oscillations for zero g in Sec. IV A and then for nonzero g in Sec. IV B.

A. Zero gravity

Figure 10 compares the results obtained with and without oscillations in zero g. We observe the following effects of oscillations:

- Figure 10(a) shows that a higher frequency of oscillations lifts the stress curve for lower values of Ω.
- The quadratic scaling of stress with Ω is modified at low Ω's. In this regime, the stress depends weakly on Ω. In the fast shearing regime, i.e., $\Omega>10$ rad/s, the stress scaling is close to quadratic, similar to the nonoscillating case. A smooth transitional regime, without well defined scaling, is

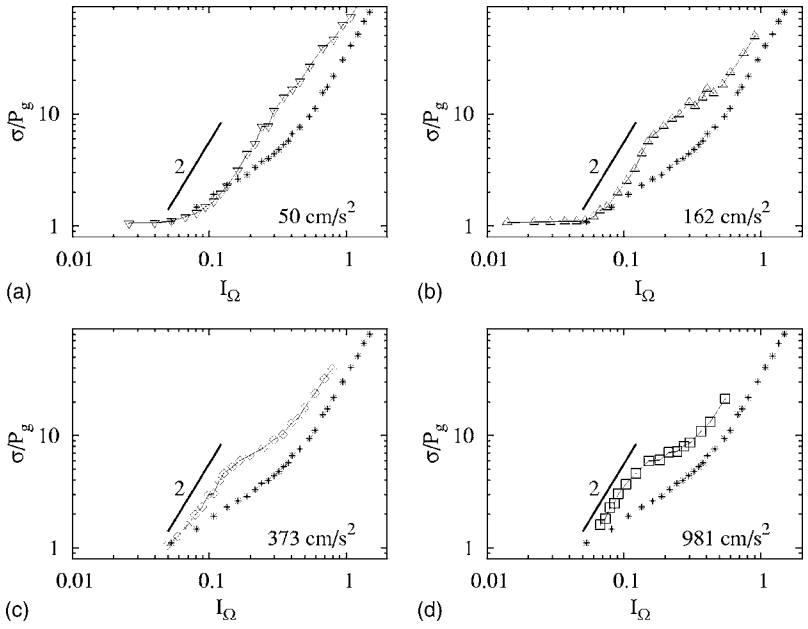

FIG. 11. Dimensionless normal stress versus I_Ω in the presence of bottom wall oscillations: (a) $g=50$ cm/s^2, (b) $g=162$ cm/s^2, (c) $g=373$ cm/s^2, and (d) $g=981$ cm/s^2. The results obtained in the systems without oscillations are replotted here from Fig. 4 (asterisks).

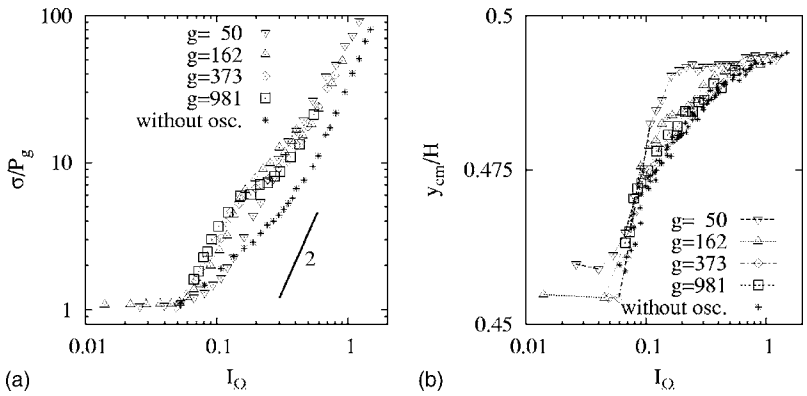

FIG. 12. (a) Dimensionless stress versus I_Ω for the systems with oscillations. (b) y position of the center of mass of all particles in nonzero gravities.

observed for intermediate values of the shearing.

- Figure 10(b) shows that at low shear rates, the particles are pushed away from the bottom wall by the oscillations, creating a dilation area there. This effect is also seen in the volume fraction profile in Fig. 10(c). As a result, the particles experience stronger interactions with the top wall and increased slippage at the bottom, viz. the velocity profiles shown in Fig. 10(d), resulting in a weak effect of the shear on the bottom wall stress, as shown in Fig. 10(a). As Ω increases, the center of mass, y_{cm}, approaches the bottom wall almost logarithmically with Ω, see Fig. 10(b). For Ω larger than some critical value, y_{cm} and the volume fraction profiles are Ω-independent. For these high Ω's, there is almost no difference between the oscillating and corresponding nonoscillating configurations, leading to similar stress scaling in both cases, as shown in Fig. 10(a). Consistently, the velocity profiles shown in Fig. 10(d) are much less sensitive to oscillations for high Ω's.
- An additional inspection of the animations of the dynamics close to the bottom wall shows that the reduced volume fraction there in the case of small Ω [see Fig. 10(c)] results in chaotic and random motions of the particles. One consequence of this behavior is the weak response of the normal stress to shear. We will see below in Sec. IV B that the presence of gravity also leads to flattening of the stress versus Ω curves, but for very different reasons.

B. Nonzero gravity

Figure 11 shows the dimensionless stress σ_{yy}/P_g versus I_Ω in nonzero gravities. In all cases, at low values of I_Ω we observe the "no-shear" state, which is characterized predominantly by the oscillating mode with nearly nonexistent shear flow. The scaled normal stress in this regime is independent of both gravity and applied shear, being essentially the gravitational weight of the system per area. We note that this oscillating mode is absent in the zero g case; therefore, the origin of the flattening of the stress versus the Ω curve is very different in the systems with nonzero g.

As I_Ω increases, we observe a transition to the "shear" regime. For larger gravities, this transition is very sharp, so that the stress almost immediately follows a quadratic scaling as I_Ω is increased. For some intermediate values of I_Ω, we note a short transitional regime with the stress scaling less than quadratically with I_Ω, and followed again by another quadratic scaling regime for high I_Ω's. The transitional regime is almost nonexistent for $g=50$ cm/s^2. The transitional regime appears to be the remnant of a linear scaling regime observed in the absence of oscillations. We find it interesting and unexpected that the oscillations preserve the linear scaling for intermediate I_Ω's, but modify the scaling back to quadratic scaling for $I_\Omega<0.15$. We note that a transition from quadratic scaling to less than quadratic scaling with an increase of shear was also observed in experiments by Savage and Sayed[16] (see, for example, Fig. 9 of the reference). Our results suggest that the above-mentioned experimental results were obtained in the setting where vibrations of the whole apparatus (possibly due to functioning of the motor drive) may have been present. Further exploration of this regime is left for future work.

Figure 12(a) shows the stresses for all nonzero gravities for both oscillated and nonoscillated systems ($f=36.6$ Hz). In this figure, we can clearly see how the interplay between oscillatory driving, shear, and gravity leads to modification of the stress scaling. For small I_Ω, the stress curves collapse as gravity increases. For larger I_Ω's, there is essentially no dependence of the scaled stresses on gravity, and the results are qualitatively similar to the ones obtained for zero g, viz. Fig. 10(a).

Figure 12(b) shows the position of the center of mass, y_{cm}. We immediately note the strong effect of gravity [compare with Fig. 10(b) for $g=0$ results]. In both cases (zero or nonzero g), a similar value is reached for larger values of I_Ω; however, in the case of zero g this limit is approached from above, and for nonzero g it is approached from below. As expected, similar behavior is reached for large I_Ω, since in this regime shearing is the dominant force in the system and

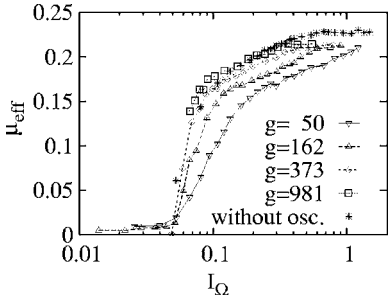

FIG. 13. Ratio of shear to normal stress, μ_{eff}, for nonzero gravities.

TABLE I. Studied Γ's and corresponding gravities and frequencies.

Γ	0.01	0.01	0.10	0.10	0.54	0.90	1.42	2.00	2.00	3.27	5.31	10.58
g(cm/s^2)	981	373	162	373	981	50	373	50	162	162	50	50
f (Hz)	5.1	3.2	6.4	9.7	36.6	10.7	36.6	15.9	28.6	36.6	25.9	36.6

the exact value of g is not important. We note that for small gravity, $g=50$ cm/s^2, y_{cm} increases to its maximum value at much lower I_Ω compared to larger gravities.

Figure 13 shows the ratio of shear to normal stress (effective friction, μ_{eff}), as a function of I_Ω. By comparison to the results obtained without oscillations from Fig. 7 (and replotted here), we note that the oscillations significantly modify μ_{eff} for small and intermediate values of I_Ω; in particular, the values obtained using different values of g do not collapse onto the same curve, as was observed for the nonoscillated system. The increase of μ_{eff} as I_Ω increases is slower for smaller values of g.

C. Dependence on oscillation parameters

We have so far introduced one dimensionless parameter, I_Ω, which can be also thought of as a ratio of relevant time scales and/or relevant velocity scales introduced into the system by shear and by gravity. The addition of oscillations introduces an additional time and velocity scale into the system, which requires an additional independent dimensionless parameter to characterize the flow. Here we follow a slightly different route and compare relevant *accelerations* introduced in the problem by gravity and vibrations, and analyze whether this nondimensional acceleration

$$\Gamma = \frac{a(2\pi f)^2}{g} \tag{6}$$

can be used to successfully correlate some flow features presented in the previous sections. Specifically, we explore the effect of Γ on the stress scaling and other properties of the granular flow. With fixed amplitude of the oscillations, a, we vary both g and f to obtain the results for the range of Γ's listed in Table I.

Figure 14 shows the collapse of the calculated stresses for fixed Γ. Each panel of the figure shows that different (g,f) pairs that lead to the same Γ result in the same stress versus I_Ω curves. Therefore, Γ seems to be an appropriate quantity to characterize the effect of oscillations on the stress scaling, and we may attempt to describe the granular dynamics in terms of two nondimensional parameters, Γ and I_Ω.

Figure 15 shows the stress scaling for different Γ's: small values ($\Gamma<1$) are shown in Fig. 15(a) and large ones ($\Gamma>1$) in Fig. 15(b) (only some representative results from the list given in the Table I are shown here). First, we note that for the smallest considered Γ, $\Gamma=0.01$, the stress scaling is similar to the nonoscillating system (marked with asterisks in Fig. 15), i.e., we have linear scaling at low I_Ω followed by quadratic scaling at higher I_Ω. However, even for such a small $\Gamma=0.01$, the stresses are significantly larger compared to the $\Gamma=0$ case of no oscillations. Therefore, we conjecture that oscillations play the role of a "singular perturbation" in sheared granular systems under gravity.

As Γ increases toward $\Gamma=1$, the most notable feature of the results shown in Fig. 15(a) is a modification of the stress scaling for small values of I_Ω from approximately linear to approximately quadratic. Further increases of Γ lead, perhaps surprisingly, to a reverse trend of the stress curves in the case of slow shear, see Fig. 15(b). Here we observe a decrease of the scaled stress as Γ is increased. This effect can be explained by noting that in the case of large Γ, the system is expected to show similar behavior as in the case of zero g. The zero g case is, for small I_Ω, characterized by slower than quadratic scaling of the stress with Ω, see Fig. 10(a). This modification of the stress scaling is responsible for an effective decrease of the normal stress as Γ is increased.

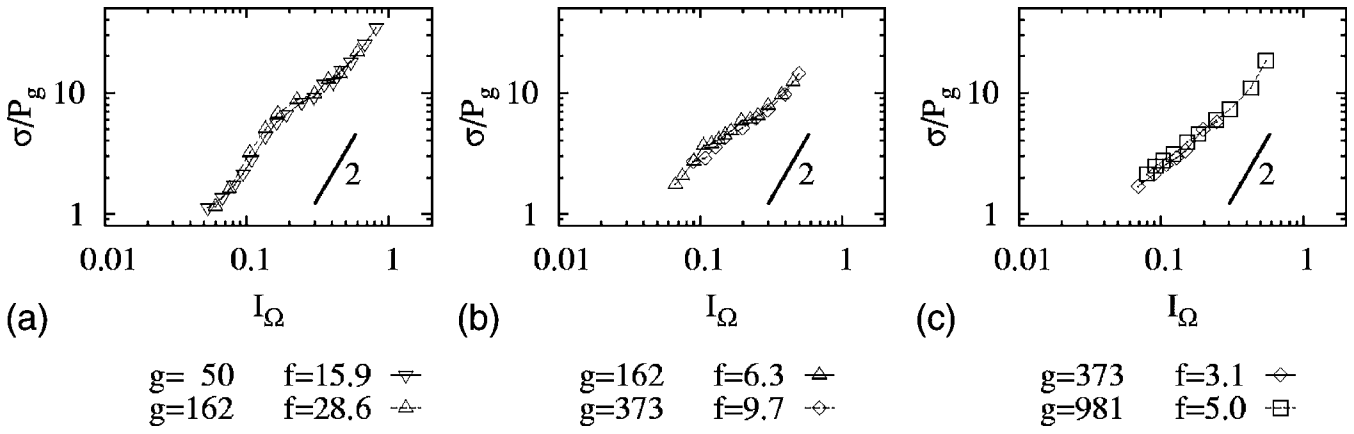

FIG. 14. Normal stress versus I_Ω for various combinations of g's and f's, leading to the same value of Γ: (a) $\Gamma=2$, (b) $\Gamma=0.1$, and (c) $\Gamma=0.01$.

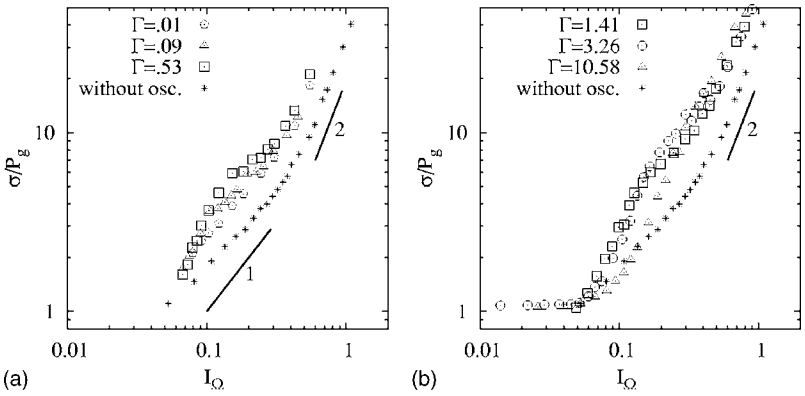

FIG. 15. Stress scaling for different Γ's.

V. CONCLUSIONS

We have studied the effect of gravity on granular systems exposed to shear and oscillations. In the case with no oscillations, we find that an excellent description can be obtained with a help of a dimensionless "inertial number" I_Ω [Eq. (4)], which depends on the applied shear rate and gravity. We show that, as I_Ω reaches values of O(1), the overall stress on the bottom boundary exhibits a transition from a linear to a quadratic scaling regime as a function of the imposed shear rate.

In the systems exposed to oscillations in addition to shear, a useful description of the flow can be obtained by using an additional nondimensional parameter, $\Gamma = a(2\pi f)^2/g$, which measures the strength of the oscillations relative to gravity. One perhaps surprising result is that even very weak oscillations lead to a significant modification of the values of the stresses in the system. However, the scaling of the stresses with shear rate obtained for $\Gamma = 0$ is retrieved in the $\Gamma \to 0$ limit. As Γ increases and reaches values of O(1), we find that the scaling of the stress with the shear rate is characterized by two approximately quadratic regimes separated by an intermediate slower-than-quadratic scaling regime. The details of the stress versus strain curve in this intermediate regime are still to be explored in more detail. For large Γ, this intermediate linear regime is absent and the stress/strain curve looks more similar to the $g=0$ ($\Gamma = \infty$) case. The $g=0$ case is characterized, however, by additional characteristics, such as dilation at the bottom wall.

ACKNOWLEDGMENTS

We acknowledge the support of NASA, Grant No. NNC04GA98G. We thank Robert P. Behringer, Deniz Ertas, Paul Mort, and Allen Wilkinson for useful discussions and comments.

[1] B. Miller, C. O'Hern, and R. P. Behringer, "Stress fluctuations for continuously sheared granular materials," Phys. Rev. Lett. **77**, 3110 (1996).
[2] M. Alam, V. H. Arakeri, P. R. Nott, J. D. Goddard, and H. J. Herrmann, "Instability-induced ordering, universal unfolding and the role of gravity in granular Couette flow," J. Fluid Mech. **523**, 277 (2005).
[3] S. B. Savage, "Analyses of slow high-concentration flows of granular materials," J. Fluid Mech. **377**, 1 (1998).
[4] C. S. Campbell, "Granular shear flows at the elastic limit," J. Fluid Mech. **465**, 261 (2002).
[5] Y. Zhang and C. S. Campbell, "The interface between fluid-like and solid-like behaviour in two-dimensional granular flows," J. Fluid Mech. **237**, 541 (1992).
[6] O. Baran and L. Kondic, "Velocity profiles, stresses, and Bagnold scaling of sheared granular system in zero gravity," Phys. Fluids **17**, 073304 (2005).
[7] C. R. Wassgren, M. L. Hunt, P. J. Freese, J. Palamara, and C. E. Brennen, "Effects of vertical vibration on Hopper flows of granular material," Phys. Fluids **14**, 3439 (2002).
[8] E. R. Nowak, J. B. Knight, E. Ben-Naim, H. M. Jaeger, and S. R. Nagel, "Density fluctuations in vibrated granular materials," Phys. Rev. E **57**, 1971 (1998).
[9] A. Prados, J. J. Brey, and B. Sanchez-Rey, "Hysteresis in vibrated granular media," Physica A **284**, 277 (2000).
[10] K. E. Daniels and R. P. Behringer, "Hysteresis and competition between disorder and crystallization in sheared and vibrated granular flow," Phys. Rev. Lett. **94**, 168001 (2005).
[11] R. A. Bagnold, "Experiments on a gravity-free dispersion of large solid spheres in a Newtonian fluid under shear," Proc. R. Soc. London, Ser. A **225**, 49 (1954).
[12] G. I. Tardos, S. McNamara, and I. Talu, "Slow and intermediate flow of a frictional bulk powder in the Couette geometry," Powder Technol. **131**, 23 (2003).
[13] P. A. Thompson and G. S. Grest, "Granular flow: Friction and the dilatancy transition," Phys. Rev. Lett. **67**, 1751 (1991).
[14] F. da Cruz, S. Emam, M. Prochnow, J.-N. Roux, and F. Chevoir, "Rheophysics of dense granular materials: Discrete simulation of plane shear flows," Phys. Rev. E **72**, 021309 (2005).
[15] G. D. R. MiDi, "On dense granular flows," Eur. Phys. J. E **14**, 341 (2004).
[16] S. B. Savage and M. Sayed, "Stresses developed by dry cohesionless granular materials sheared in an annular shear cell," J. Fluid Mech. **142**, 391 (1984).
[17] C. Bizon, M. D. Shattuck, J. B. Swift, W. D. McCormick, and H. L. Swinney, "Patterns in 3D vertically oscillated granular layers: Simulation and experiment," Phys. Rev. Lett. **80**, 57 (1998).
[18] O. R. Walton, in *Particulate Two-phase Flow*, edited by M. C. Roco (Butterworth-Heinemann, Boston, 1993), p. 884.
[19] More information and animations of the flow in zero g can be found at http://m.njit.edu/~oleh/shear_shake/, or by contacting the authors.
[20] A. W. Lees and S. F. Edwards, "The computer study of transport processes under extreme conditions," J. Phys. C **5**, 1921 (1972).
[21] C. S. Campbell and C. E. Brennen, "Computer simulation of granular shear flows," J. Fluid Mech. **151**, 167 (1985).
[22] O. Pouliquen, C. Cassar, Y. Forterre, P. Jop, and M. Nicolas, "How do grains flow: Towards a simple rheology for dense granular flows," in *The Proceedings of the Fifth Powders and Grains International Conference on the Micromechanics of Granular Media. Powders and Grains*, edited by R. García-Rojo, H. J. Herrmann, and S. McNamara (A. A. Balkema, Rotterdam, 2005).
[23] O. Pouliquen, "Scaling laws in granular flows down rough inclined planes," Phys. Fluids **11**, 542 (1999).